

On the Connection Between Spiral Arm Pitch Angle and Galaxy Properties

SI-YUE YU^{1,2} AND LUIS C. HO^{1,2}

¹*Kavli Institute for Astronomy and Astrophysics, Peking University, Beijing 100871, China*

²*Department of Astronomy, School of Physics, Peking University, Beijing 100871, China*

ABSTRACT

We measure the pitch angle (φ) of spiral arms in a sample of 79 galaxies to perform a systematic study of the dependence of φ on galaxy morphology, mass, and kinematics to investigate the physical origin of spiral arms. We find that φ decreases (arms are more tightly wound), albeit with significant scatter, in galaxies with earlier Hubble type, more prominent bulges, higher concentration, and larger total galaxy stellar mass (M_*^{gal}). For a given concentration, galaxies with larger stellar masses tend to have tighter spiral arms, and vice versa. We also find that φ obeys a tight inverse correlation with central stellar velocity dispersion for $\sigma_c \gtrsim 100 \text{ km s}^{-1}$, whereas φ remains approximately constant for $\sigma_c \lesssim 100 \text{ km s}^{-1}$. We demonstrate that the φ - σ_c and φ - M_*^{gal} relations are projections of a more fundamental three-dimensional φ - σ_c - M_*^{gal} relation, such that pitch angle is determined by σ_c for massive galaxies but by M_*^{gal} for less massive galaxies. Contrary to previous studies, we find that φ correlates only loosely with the galaxy's shear rate. For a given shear rate, spirals generated from N -body simulations exhibit much higher φ than observed, suggesting that galactic disks are dynamically cooler (Toomre's $Q \approx 1.2$). Instead, the measured pitch angles show a much stronger relation with morphology of the rotation curve of the central region, such that galaxies with centrally peaked rotation curves have tight arms, while those with slow-rising rotation curves have looser arms. These behaviors are qualitatively consistent with predictions of density wave theory.

Keywords: galaxies: kinematics and dynamics – galaxies: photometry – galaxies : spiral – galaxies: structure

1. INTRODUCTION

Spiral structures are the most prominent features of disk galaxies, but their physical origin is still debated. Pitch angle (φ), defined as the angle between the tangent of the spiral and the azimuthal direction, describes the degree of tightness of a spiral arm (Binney & Tremaine 2008).

As the tightness of spiral arms constitutes one of the essential criteria of Hubble's scheme of morphological classification of galaxies (Hubble 1926; Sandage 1961), the pitch angle of spiral arms tends to decrease (become more tightly wound) from late to early Hubble types (Kennicutt 1981; Ma 2002; Yu et al. 2018). Density wave theory (Lin & Shu 1964; Bertin et al. 1989a,b; Bertin & Lin 1996) offers the most successful framework to explain spiral structures. The semi-empirical study of Roberts et al. (1975) showed that density wave theory can fit observed spiral arms and suggested that mass concentration is the main determinant of spiral arm pitch angle. By constructing appropriate basic states of galaxy models, Bertin et al. (1989a) numerically cal-

culated density wave modes that are able to represent all Hubble types and confirmed that spiral arms become tighter with increasing mass fraction in the central spherical component. A number of studies have used other lines of evidence to argue in favor of density wave theory, in terms of the classic aging of the stellar population that produces a color gradient across spiral arms (Gonzalez & Graham 1996; Martínez-García et al. 2009a; Martínez-García & González-Lópezlira 2011; Yu & Ho 2018) and the dependence of pitch angle on wavelength predicted by Gittins & Clarke (2004) (Martínez-García 2012; Martínez-García & González-Lópezlira 2013; Martínez-García et al. 2014; Yu & Ho 2018).

In contrast, N -body simulations of isolated pure stellar disk galaxies generate spiral arms as transient but recurrent structures (Carlberg & Freedman 1985; Bottenga 2003; Sellwood 2011; Fujii et al. 2011; Grand et al. 2012a,b; Baba et al. 2013; D'Onghia et al. 2013). In these simulations, the tendency for the number of arms to increase with decreasing disk mass fraction and for the pitch angle to increase with decreasing velocity shear are roughly consistent with the predictions

of swing amplification theory (Julian & Toomre 1966; Goldreich & Tremaine 1978; Toomre 1981). In this picture, wherein spirals are transient, the pitch angle reflects the effects of differential rotation alone.

Within this backdrop, it is instructive to elucidate in a quantitative manner how spiral arm pitch angle relates to various galaxy properties. Many attempts have been made, with mixed results. Pitch angles of spiral arms were found to correlate strongly with maximum rotation velocity (Kennicutt 1981) and mean rotation velocity over the region containing spiral arms (Kennicutt & Hodge 1982), with larger rotational velocities leading to more tightly wound arms. The more recent analysis of Kendall et al. (2015), however, does not support this, although their sample contains only 13 objects. Similarly, Kennicutt (1981) found that pitch angle decreases with brighter absolute magnitude. Kennicutt (1981) further noted a correlation between pitch angle and Morgan’s (1958, 1959) classification, which is primarily based on subjective estimates of bulge-to-disk ratio, such that galaxies with larger bulge fraction tending to have smaller pitch angle, but with considerable scatter. Paradoxically, this trend is not corroborated when concentration index is used as a proxy of concentration of mass (Seigar & James 1998; Kendall et al. 2015). Seigar et al. (2005, 2006) reported a tight connection between pitch angle and morphology of the galactic rotation curve, quantified by the shear rate, with open arms associated with rising rotation curves and tightly wound arms connected to flat and falling rotation curves. On the other hand, Kendall et al. (2015) disputed the tightness of the correlation. Furthermore, Yu et al. (2018) show that about 1/3 of the pitch angles in Seigar et al. (2006) have been severely overestimated; the remeasured pitch angles correlate with shear rate weakly at best. The pitch angle of spiral arms is also found to be correlated strongly with the galaxy’s central stellar velocity dispersion, and hence with black hole mass (Seigar et al. 2008), by virtue of the well-known relation between black hole mass and bulge stellar velocity dispersion (see Kormendy & Ho 2013, and references therein). Lastly, to round off this list of confusing and often contradictory results, Hart et al. (2017) analyzed a large sample of galaxies selected from the Sloan Digital Sky Survey (SDSS; York et al. 2000) and found very weak correlations between pitch angle and galaxy mass, but the surprising trend that pitch angle increases with increasing bulge-to-total mass ratio.

The morphology of spiral arms may depend on wavelength. Weak, two-arm spirals had been seen in some flocculent galaxies (Block et al. 1994; Thornley 1996; Thornley & Mundy 1997; Elmegreen et al. 1999;

Block & Puerari 1999). Still, pitch angles measured in the near-infrared generally agree well with those measured in the optical (Seigar et al. 2006; Davis et al. 2012). The recent study by Yu & Ho (2018) report a mean difference in pitch angle of only $\sim 0.5^\circ$ between spiral arms observed in $3.6\mu\text{m}$ and R -band images, which lays the foundation for our use of SDSS r -band images to measure pitch angle in this paper.

The Calar Alto Legacy Integral Field Area (CALIFA) survey (Sánchez et al. 2012) targets a diameter-limited sample of galaxies covering all morphological types, in the redshift range $0.005 < z < 0.03$. For these low redshifts, SDSS provides images of adequate quality for measuring pitch angle (Yu et al. 2018). Falcón-Barroso et al. (2017) extracted stellar kinematic maps of 300 CALIFA galaxies using the PPF fitting procedure (Cappellari & Emsellem 2004). From this original sample, after discarding galaxy mergers and cases with uncertain dynamical models, Kalinova et al. (2017) derived circular velocity curves for 238 objects using detailed stellar dynamical Jeans modeling (Cappellari 2008). Other galaxy properties, such as stellar masses, photometric decomposition, and star formation rates are also available (Walcher et al. 2014; Sánchez et al. 2016, 2017; Méndez-Abreu et al. 2017; Catalán-Torrecilla et al. 2017; Gilhuly & Courteau 2018). This database enables us to perform a comprehensive study of the dependence of spiral arm pitch angle on various galaxy properties.

2. DATA

We select our galaxies from the sample of Kalinova et al. (2017), who provide rotation curves of 238 CALIFA galaxies, which can be used to derive velocity shear rates. We use their corresponding SDSS r -band images to analyze their spiral arms. We visually inspect the images to exclude ellipticals, edge-on disks, and irregular systems, finally settling on 93 nearly face-on galaxies having spiral structure. We then generate a mask to exclude foreground stars and produce star-cleaned images following the procedures described in Ho et al. (2011). The background level was determined from 10 randomly selected empty sky regions and then subtracted from the star-cleaned images. As shown in the next section, we successfully measured pitch angles for 79 of the 93 galaxies. The distribution of Hubble types for the final sample of 79 galaxies is shown in Figure 1 (red-hatched histograms), which is compared with the sample of 238 galaxies of (blue-hatched histograms; Kalinova et al. 2017). The Hubble types come from the CALIFA team (Walcher et al. 2014). The subsample of 79 galaxies well represents the distribution of Hubble types of the parent

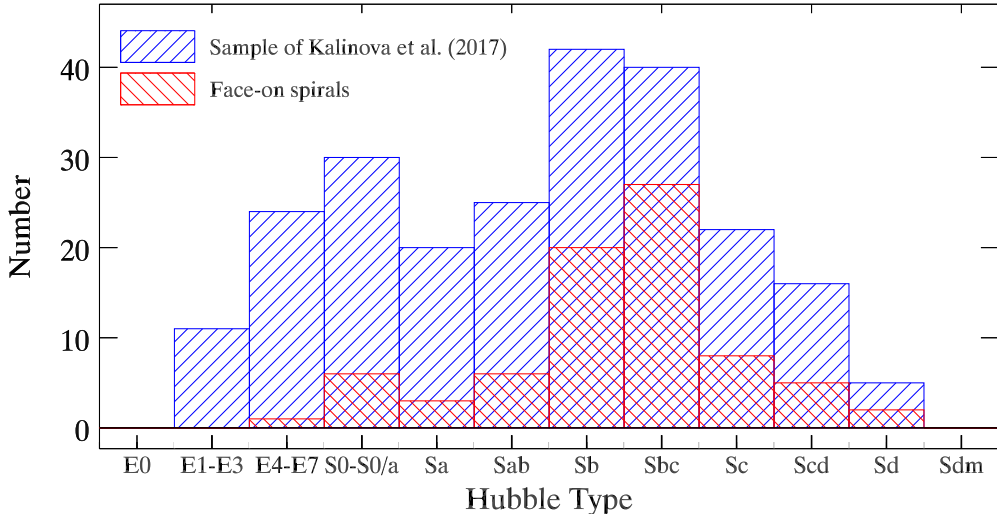


Figure 1. Distribution of Hubble types for our sample of 79 galaxies (red-hatched histograms) compared with the sample of 238 objects in Kalinova et al. (2017) (blue-hatched histograms). Our sample spans the full range of Hubble types of disk galaxies, even including an elliptical, which actually has weak but detectable spiral arms.

sample from Kalinova et al. (2017); it even includes an elliptical galaxy, which actually exhibits faint arms.

The stellar masses of the galaxies (M_*^{gal}) are from Sánchez et al. (2017), who analyzed the stellar population using the Pipe2D pipeline (Sánchez et al. 2016). Méndez-Abreu et al. (2017) performed two-dimensional multi-component photometric decomposition and characterized the main stellar substructures (bulge, bar, and disk), whose mass and star formation history were studied by Catalán-Torrecilla et al. (2017). From these studies we can compile the bulge-to-total light ratio (B/T), bulge stellar mass (M_*^{bul}), and disk stellar mass (M_*^{disk}). The uncertainty of B/T is primarily systematic in origin, driven by model assumptions instead of statistical errors from the fitting. Following (Gao & Ho 2017), we assign 10% fractional uncertainty to B/T . The concentration indices (C_{28}), derived from the isophotal analysis of Gilhuly & Courteau (2018), have fractional errors of 3%. The absolute B -band magnitudes (M_B) come from HyperLeda (Paturel et al. 2003). The central velocity dispersions (σ_c) and their uncertainties are calculated as the mean value and standard deviation of the velocity dispersion, provided by Falcón-Barroso et al. (2017), within $3''$ of the galaxy center. Kalinova et al. (2017) performed principal component analysis of the rotation curves of the CALIFA galaxies and provided the coefficient of the first eigenvector (PC_1), which quantitatively describes the shape and amplitude of the rotation curve of the central region. Section 4 shows that PC_1 is useful for our study. Table 1 lists the above-described parameters for our sample.

3. PITCH ANGLE AND SHEAR RATE

3.1. Measuring pitch angle

An accurate determination of the sky projection parameters—ellipticity (e) and position angle (PA)—for the galaxies is essential for the study of spiral arms. We adopt two methods to measure the e and PA of galaxies and determine the optimal results. One is to use the IRAF task `ellipse` to extract radial profiles of e and PA from isophotal analysis. The adopted values of e and PA are obtained by averaging their profiles in the region where the disk component dominates. The second method is to use a two-dimensional Fourier transformation of the disk region, minimizing the real part of the Fourier spectra, which corresponds to the bimodal component, to derive e and PA. These two methods assume that the disk is intrinsically circular. To determine the optimal results, we deproject the galaxies to their face-on orientation using the e and PA values from these two methods, giving preference to that which yields a rounder deprojected image or more logarithmic-shaped spiral arms. Our adopted values of e and PA are listed in Table 1.

The most widely used techniques to measure the pitch angle of spiral arms employ discrete Fourier transformation, either in one dimension (1DDFT) (Grosbøl et al. 2004; Kendall et al. 2011; Yu et al. 2018) or in two dimensions (2DDFT) (Kalnajs 1975; Iye et al. 1982; Krakow et al. 1982; Puerari & Dottori 1992; Puerari 1993; Block & Puerari 1999; Davis et al. 2012; Yu et al. 2018). Yu et al. (2018) discuss and use both techniques, in the context of images from the Carnegie-Irvine Galaxy Survey (CGS; Ho et al. 2011). As the pitch angles obtained from both methods are actually

consistent within a small scatter of 2° (Yu et al. 2018), we use 2DDFT to measure pitch angle for the majority (72/79) of our sample; the 1DDFT method was used for seven cases for which the 2DDFT method failed. In total we successfully measured pitch angles for 79 of 93 objects. Table 1 lists our pitch angle measurements, including the radial range and Fourier mode used for the calculation. Pitch angles could not be measured for the rest of the galaxies because the arms are too weak (6 galaxies), too flocculent (4 galaxies), or too wound up such that isophotes cross a single arm more than once (4 galaxies). As shown in the distribution of Hubble types in Figure 1, 20% (6) of the S0 or S0/a galaxies have very weak but detectable spiral arms whose pitch angles can be measured. An extreme case is NGC 1349, which is classified as “E” in Walcher et al. (2014) but “S0” in HyperLeda. Compared with previous studies of spiral arms that use known “spirals” as one of their selection criteria (Kennicutt 1981; Seigar & James 1998; Seigar et al. 2005, 2006; Kendall et al. 2011; Elmegreen & Elmegreen 2014), our sample is more complete by including disks in early-type galaxies with faint arms.

3.2. Measuring shear rate

The galactic shear rate (Γ), which quantifies the morphology of the rotation curve, is given by

$$\Gamma = \frac{2A}{\Omega} = 2 - \frac{\kappa^2}{2\Omega^2} = 1 - (R/V_c)(dV_c/dR), \quad (1)$$

where R is the radial distance from the center, V_c is the circular velocity, A is first Oort constant, Ω is angular speed, and κ is epicyclic frequency. Eq. (1) is the most widely adopted definition of shear rate (e.g., Bertin et al. 1989b; Grand et al. 2013; Dobbs & Baba 2014; Michikoshi & Kokubo 2014), but is 2 times the shear rate defined by Seigar et al. (2005). We use the rotation curves of Kalinova et al. (2017) to derive Γ .

We first identify an outer region that is beyond the turnover of the rotation curve ($[r_i, r_o]$), one that preferably coincides with the radial region used to derive the pitch angle. For a few galaxies whose radial region occupied by spiral arms exceeds the radial extent of the rotation curve, we choose the outer region where the rotation curve has become stable. To evaluate Γ , we fit the function

$$V_c = b \times e^{(1-\Gamma)\ln R}, \quad (2)$$

where b is a coefficient, to the rotation curve in three radial ranges: $[r_i, r_o - \Delta r]$, $[r_i + \Delta r, r_o]$, and $[r_i + \Delta r/2, r_o - \Delta r/2]$,

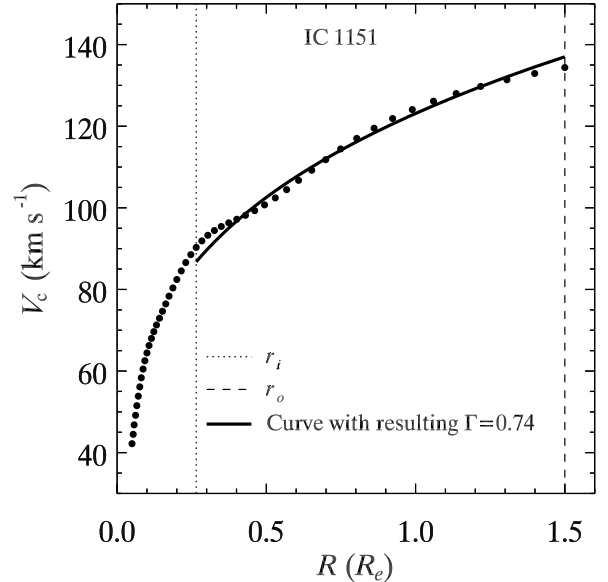


Figure 2. Example of measuring shear rate for IC 1151. Three radius ranges: $[r_i, r_o - \Delta r]$, $[r_i + \Delta r, r_o]$, and $[r_i + \Delta r/2, r_o - \Delta r/2]$, where $\Delta r = 0.2(r_o - r_i)$, are used to fit the function in Equation (2). The solid line represents the function with averaged Γ and b .

$\Delta r/2]$, where $\Delta r = 0.2(r_o - r_i)$. The value of Γ and its uncertainty (Table 1), introduced from the choice of radial range, are estimated as the mean value and standard deviation of the three values of Γ obtained from the fitting over the above three radial ranges.

Figure 2 gives an illustration for IC 1511, for which the filled points represent the rotation curve and the solid line marks the curve that yields a shear rate of $\Gamma = 0.74$. Note that when $\Gamma = 1$, the outer part of the rotation curve is flat; when $\Gamma < 1$, the outer part of the rotation curve is rising; when $\Gamma > 1$, the outer part of the rotation curve is falling.

4. THE RELATIONSHIP BETWEEN PITCH ANGLE AND GALAXY PROPERTIES

In this section, we study the dependence of spiral arm pitch angle on various galaxy properties (morphology, luminosity, stellar mass, and kinematics), and then compare our findings with previous studies, which sometimes reveal conflicting results.

4.1. Dependence on Galaxy Morphology

Hubble types are subjective. Different classifications place different weights on the classification criteria and may lead to different results. To assess the uncertainty of the Hubble types of our sample, we compare the types determined by Walcher et al. (2014) with those given in HyperLeda (Paturel et al. 2003): the two are consistent

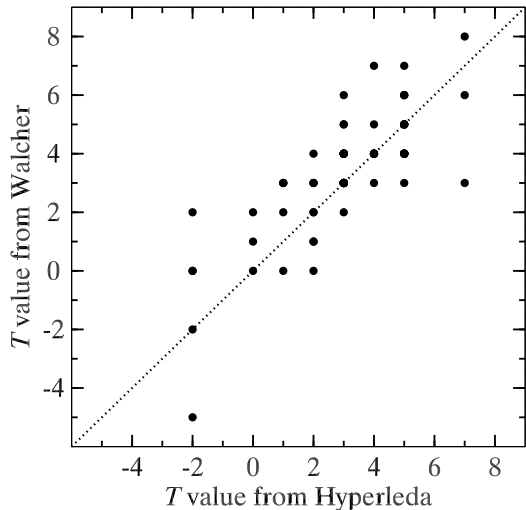


Figure 3. Comparison between Hubble type of our sample, adopted from Walcher et al. (2014), with classifications given in Hyperleda (Paturel et al. 2003). The correspondence between Hubble type and T value is as follows: E: $T = -5$; S0: $T = -2$; S0/a: $T = 0$; Sa: $T = 1$; Sab: $T = 2$; Sb: $T = 3$; Sbc: $T = 4$; Sc: $T = 5$; Scd: $T = 6$; Sd: $T = 7$; Sdm: $T = 8$; Sm: $T = 9$. The dotted line mark the 1 : 1 ratio. The Hubble types from these two sources are roughly consistent with a total scatter in T value of $\sigma_T = 1.3$.

within a scatter of $\sigma_T = 1.3$ in T (Figure 3). The measured pitch angle of spiral arms is plotted against Hubble type determined by Walcher et al. (2014) in Figure 4a, where the open points mark the mean value and associated errors. The uncertainty of the mean Hubble type is determined by σ_T/\sqrt{N} , with N the number of objects in each Hubble type bin. Despite the fact that our sample contains fewer early-type spirals than late-type spirals, our results confirm that on average spiral arms tend to be more tightly wound in galaxies of earlier Hubble type, but with large scatter in pitch angle ($\sim 7^\circ$). Most of the early-type spirals (Sab and earlier) have pitch angles less than 15° , while later type spirals (Sb and later) can have both high ($\sim 30^\circ$) and low ($\sim 10^\circ$) pitch angles. This behavior is not entirely consistent with the Hubble classification system, which implicitly considers tightness of spiral arms. Part of the scatter in the relation between pitch angle and Hubble type may come from the subjective nature of morphological classification. However, repeating the analysis using Hubble types from Hyperleda (Paturel et al. 2003) yields very similar results (Figure 4b), indicating that a large portion of scatter in pitch angle at a given Hubble type is real. Studies by Kennicutt (1981) and Ma (2002) also found a weak correlation between pitch angle and Hubble type, with large scatter in pitch angle at a given type.

But such a trend was not seen by Kendall et al. (2015), probably because of their small sample of just 13 objects, nor by Seigar & James (1998), probably because nearly all of their pitch angles were less than 15° .

Density wave theory predicts an inverse correlation between pitch angle and mass concentration (Lin & Shu 1964; Roberts et al. 1975; Bertin et al. 1989a,b). The relative prominence of the bulge, as reflected, for instance, in the bulge-to-total light ratio (B/T), should provide a reasonable proxy for the stellar mass concentration. The same holds for the concentration parameter $C_{28} \equiv R_{80}/R_{20}$, with R_{20} and R_{80} the radii enclosing, respectively, 20% and 80% of the total flux. Figure 5 shows the relation between pitch angle φ and B/T and C_{28} . We group the data points into five equal-sized bins of B/T and C_{28} , and then calculate the mean value and standard deviation of each bin. The number of bins is set to ensure sufficient sampling. In general, φ decreases with increasing B/T and C_{28} , with Pearson correlation coefficients of $\rho = -0.28$ and $\rho = -0.46$, respectively, although the scatter is substantial. These results are at odds with the conclusions of Hart et al. (2017), who reported a slight tendency for φ to rise with increasing ratio of bulge mass to total mass, precisely the *opposite* of what we see. Contrary to previous studies (Seigar & James 1998; Kendall et al. 2015), we find a significant correlation between φ and C_{28} : φ decreases from $= 23^\circ.7 \pm 4^\circ.8$ at $C_{28} = 2.0 \pm 0.2$ to $13^\circ.4 \pm 6^\circ.1$ at $C_{28} = 5.0 \pm 0.2$. The marked scatter in the $\varphi - B/T$ diagram may stem, in part, from the many complications in bulge-to-disk decomposition (Gao & Ho 2017). Our results imply that galaxies with more centrally concentrated mass distributions tend to have more tightly wound spiral arms.

4.2. Dependence on Luminosity and Mass

Figure 6 examines the variation of pitch angle with absolute B -band magnitude (M_B), total galaxy stellar mass (M_*^{gal}), and separately the stellar mass of the bulge (M_*^{bul}) and disk (M_*^{disk}). The results from Hart et al. (2017), marked by the orange line, are shown for comparison. As shown in Figure 6, the distributions of the data are not homogenous, and there are fewer data points in the faint, low-mass end. Thus, we manually adjust the number of objects in the first bin to include all sources up to $M_B = -19.3$, $M_*^{\text{gal}} = 10^{10} M_\odot$, $M_*^{\text{bul}} = 10^8 M_\odot$, and $M_*^{\text{disk}} = 10^{10} M_\odot$, and the rest of the data were further grouped into four equal-sized bins. The binned data support the notion that more luminous, more massive galaxies tend to have more tightly wound spiral arms (smaller values of φ). The apparent bimodal distribution at $M_B \approx -20.7$ mag is proba-

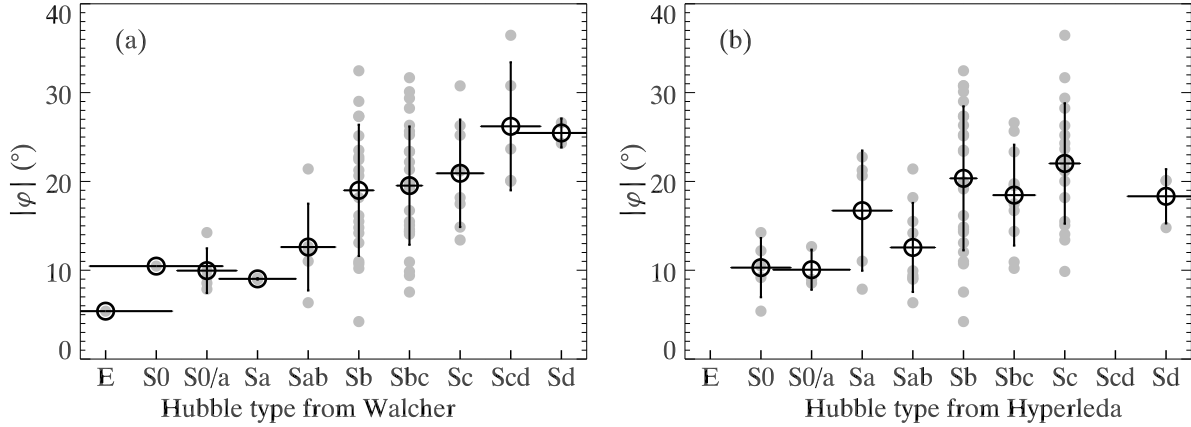


Figure 4. Variation of spiral arm pitch angle with Hubble type from (a) Walcher et al. (2014) and (b) Hyperleda (Paturel et al. 2003). The large open points mark the mean value and associated errors. The uncertainty of the mean Hubble type is determined by σ_T/\sqrt{N} , with N the number of objects in each Hubble type bin. Most of the scatter in pitch angle for a given Hubble type is real and not caused by subjective classification.

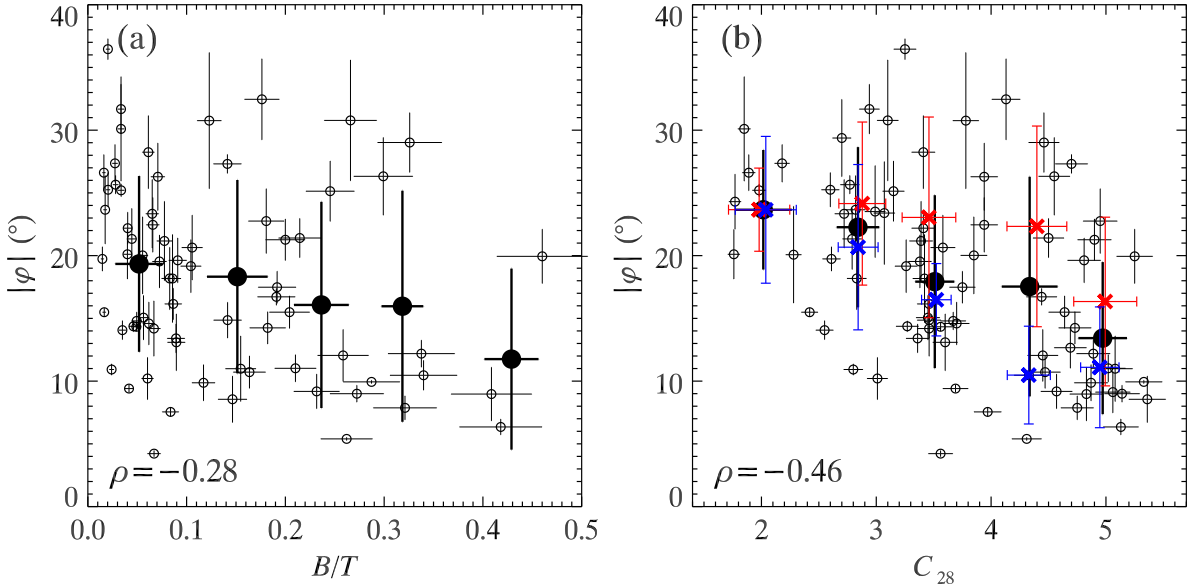


Figure 5. Variation of pitch angle of spiral arms with (a) bulge-to-total light ratio B/T and (b) concentration index C_{28} . The data points are separated into five equal-sized bins of B/T or C_{28} . The mean value and standard deviation of each bin is marked by solid black points and associated error bars. Pitch angle correlates weakly with B/T and somewhat stronger with C_{28} . For each of the five bins of C_{28} , the data are further separated into two subsets according to the mean value of M_*^{gal} ; the mean and standard deviation of the subset above and below the mean are marked by the blue and red crosses, respectively. The Pearson's correlation coefficient, ρ , is shown on the bottom-left of each panel.

bly an artifact of the small number of data points in the range from 8° to 32° . The correlation between φ and M_B is mainly driven by the close coupling between M_B and M_*^{gal} . The measured pitch angles decrease from $\varphi = 26^\circ \pm 5^\circ.9$ at $\log(M_*^{\text{gal}}/M_\odot) = 9.6 \pm 0.2$ to $\varphi = 13^\circ.8 \pm 5^\circ.3$ at $\log(M_*^{\text{gal}}/M_\odot) = 11.1 \pm 0.1$. Similarly, pitch angles decrease toward larger M_*^{bul} and M_*^{disk} , with scatter comparable to that of the $\varphi - M_*^{\text{gal}}$ relation. The apparent flattening or even reversal toward

the lowest mass bin is probably caused by insufficient sampling. As illustrated by the orange lines, Hart et al. (2017) find essentially no relationship between pitch angle and stellar mass (total, bulge, or disk), and at a given mass their pitch angles are systematically smaller than ours. The discrepancy is likely caused by the usage of different techniques to measure pitch angle. The Fourier transformation we employ uses flux as weighting when calculating Fourier spectra, and so it tends

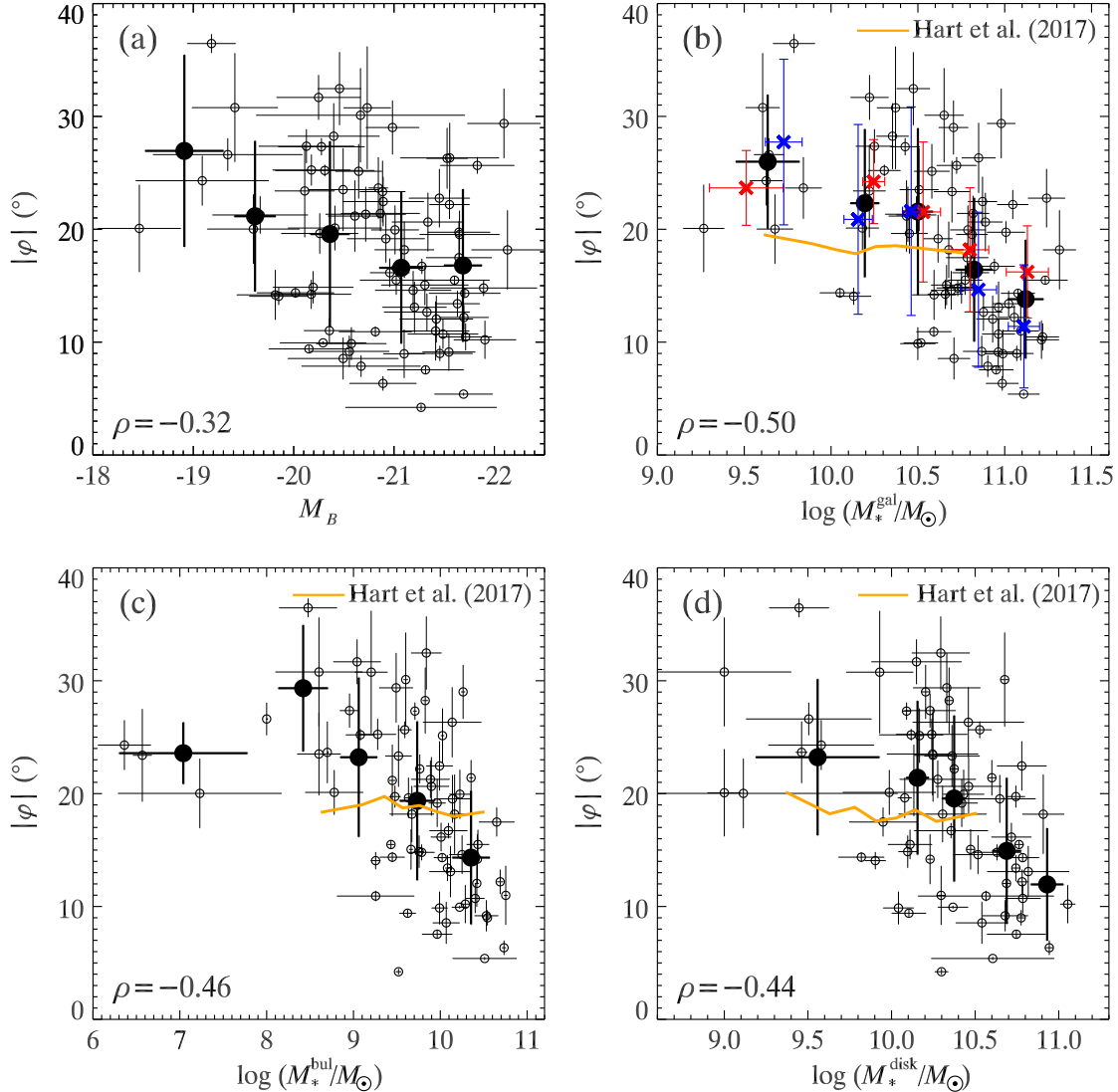


Figure 6. Dependence of pitch angle on (a) absolute B -band magnitude (M_B), (b) galaxy stellar mass (M_*^{gal}), (c) bulge stellar mass (M_*^{bul}), and (d) disk stellar mass (M_*^{disk}). The solid black points and their associated error bars mark the mean value and standard deviation of the data in each of the five bins of the parameter on the X-axis value. To obtain sufficient data points, the number of objects in the first bin was manually adjusted to include all sources up to $M_B = -19.3$, $M_*^{\text{gal}} = 10^{10} M_\odot$, $M_*^{\text{bul}} = 10^8 M_\odot$, and $M_*^{\text{disk}} = 10^{10} M_\odot$, and the rest of the data were further grouped into four equal bins. Results from Hart et al. (2017) are marked by orange lines, which show a nearly flat trend. For each of the five bins of M_*^{gal} , the data are further separated into two subsets according to the mean value of C_{28} ; the mean and standard deviation of the subset above and below the mean are marked by the blue and red crosses, respectively. The Pearson’s correlation coefficient, ρ , is shown on the bottom-left of each panel.

to extract information from the dominant modes of the spiral structure. Hart et al. (2017), by contrast, employ the code SpArcFiRe (Davis & Hayes 2014), which uses texture analysis to identify arc-like segments, including very faint arms, and then averages the pitch angles of these segments, weighting by their length. However, the faint arms, whose physical significance is unclear, may adversely affect their final measurement of pitch angle.

Our findings are qualitatively consistent with the theoretical expectations of density wave theory. Roberts et al. (1975) argued that the mass concentration determines the pitch angle of spiral arms, a conclusion confirmed by the modal analysis of Bertin et al. (1989a). In a similar vein, Hozumi (2003) suggested that tighter spiral arms are associated with higher surface density. In Figure 6b, we study the effect of mass concentration on arm tightness at *fixed* galaxy mass, by grouping

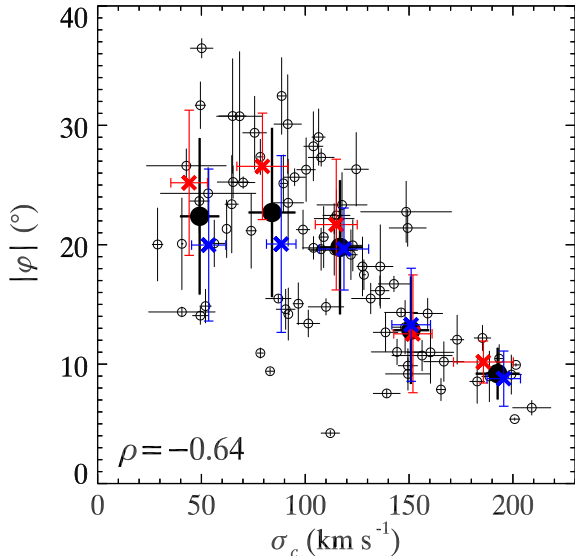


Figure 7. Correlation between pitch angle and central velocity dispersion (σ_c). The data points are grouped into five equal bins of σ_c . The solid black points and their associated error bars mark the mean value and standard deviation of the data in each bin. The pitch angle decreases with increasing σ_c , with small scatter for $\sigma_c \gtrsim 100 \text{ km s}^{-1}$, but for $\sigma_c \lesssim 100 \text{ km s}^{-1}$ the mean value of pitch angle remains roughly constant. For the the five bins of σ_c , the data points are further separated into two parts according to the mean value of $\log(M_*^{\text{gal}})$; the mean and standard deviation of the top and bottom parts are marked by the blue and red crosses, respectively. The Pearson’s correlation coefficient, ρ , is shown on the bottom-left corner.

the data into bins of $\log(M_*^{\text{gal}})$ after dividing the sample into two subsets according to their mean value of C_{28} . For a given stellar mass $\log(M_*^{\text{gal}}/M_\odot) \gtrsim 10.4$, we note that galaxies with higher C_{28} (blue crosses) tend to have smaller φ , but the tendency disappears for stellar masses $\log(M_*^{\text{gal}}/M_\odot) \lesssim 10.4$, likely due to small number statistics. At the same time, at fixed C_{28} more massive galaxies tend to have tighter arms; the difference decreases with decreasing C_{28} and vanishes at $C_{28} \approx 2$ (Figure 5b).

4.3. Dependence on Galaxy Kinematics

4.3.1. Central velocity dispersion

Figure 7 plots pitch angles versus the central velocity dispersion (σ_c). The correlation is strong, with with Pearson correlation coefficient $\rho = -0.64$. For galaxies with $\sigma_c \gtrsim 100 \text{ km s}^{-1}$, pitch angle decreases with σ_c with small scatter, reaching a mean value of $\varphi = 9:2^\circ \pm 2:2$ at $\sigma_c = 193 \pm 11 \text{ km s}^{-1}$, the highest velocity dispersion covered by our sample. No galaxies with high σ_c show open spiral arms. By contrast, galaxies with $\sigma_c \lesssim 100 \text{ km s}^{-1}$

host arms with a wide spread in pitch angles, from values as high as $\varphi \approx 30^\circ$ to as low as $\varphi \approx 15^\circ$. The pitch angle seems to remain at a roughly constant mean value of $\varphi \approx 23^\circ$ for $\sigma_c \lesssim 100 \text{ km s}^{-1}$.

4.3.2. Comparison with previous results

Seigar et al. (2008) reported a strong inverse correlation between spiral arm pitch angle central stellar velocity dispersion for a sample of 27 galaxies. Here, we independently reexamine their results. Instead of using the same images used in Seigar et al. (2008), we use, whenever possible, images of higher quality: seven images from CGS (Ho et al. 2011), 16 images from SDSS, and three images collected from the NASA/IPAC Extragalactic Database (NED)¹. The data point for the Milky Way is not included, as its pitch angle may be unreliable. We uniformly analyze all the objects, using, for consistency, the 2D Fourier transformation method. Seigar et al. (2008) did not provide the projection parameters (e and PA) for the galaxies, and so measure them following the procedure described in Section 3.1. We successfully measure pitch angles for 21 of the 26 galaxies.

Direct comparison of our new pitch angle measurements with those published by Seigar et al. (2008) reveal that a significant fraction of them (6/21) were severely and systematically overestimated (by more than 8°). Figure 8 illustrates the four cases with the most serious discrepancy, whose pitch angles were overestimated by more than 10° . The panels in left column present the unsharp-masked images overplotted with the synthetic arm with the pitch angle derived from this work (red solid line) and from the work of Seigar et al. (2008; orange dash-dotted line). The panels in the right column plot the 2D Fourier spectra, with an arrow indicating the peak chosen to derive the pitch angle. It is obvious that the synthetic arms created using our pitch angles trace the spiral arms very well, whereas those that adopt the pitch angles from Seigar et al. (2008) do not. In the extreme case of NGC 3938 (top row), Seigar et al. (2008) quoted a pitch angle of $43:4$, whereas we find $16:7$. These four galaxies have clear spiral arms and a distinctly dominant Fourier mode. Their pitch angles can be measured rather straightforwardly and unambiguously. The large discrepancies with the published values cannot arise from errors in the measurement technique.

With our updated pitch angle measurements in hand for the 21 galaxies reanalyzed by us, we redraw in Figure 9 the relation between φ and σ_c as originally pub-

¹ <http://nedwww.ipac.caltech.edu>

lished by Seigar et al. (2008), using σ_c given by those authors (their Table 1). The relationship between φ and σ_c is considerably less tight than claimed by Seigar et al. (2008), and instead closely resembles our results based on a much larger sample (Figure 7).

4.3.3. Implications

Pitch angle correlates strongly with σ_c for $\sigma \gtrsim 100 \text{ km s}^{-1}$. As σ_c is measured within the central $3''$ ($\sim 1 \text{ kpc}$ for our median sample distance of 68 Mpc), it must connect with certain global properties to influence galactic-scale spiral structure. It is well known that the luminosity of elliptical galaxies scales with stellar velocity dispersion following $L \propto \sigma^4$ (Faber & Jackson 1976), but the Faber-Jackson relation of bulges is not well-determined. It varies systematically with Hubble type (Whitmore & Kirshner 1981; Kormendy & Illingworth 1983) and between classical bulges and pseudobulges (Kormendy & Kennicutt 2004). The correlation between pitch angle and σ_c is not entirely consistent with that between pitch angle and bulge mass. The $\varphi - M_*^{\text{bul}}$ relation clearly has larger scatter than the $\varphi - \sigma_c$ relation, especially at the high-mass end (Figure 6c). For $\sigma_c \lesssim 100 \text{ km s}^{-1}$, the mean value of pitch angle remains essentially constant, suggesting that in this regime another parameter determines the pitch angle. In order to study the effect of galaxy mass on pitch angle for a given central velocity dispersion, for each of the five bins of σ_c , we again split the data into two subsets according to the mean value of $\log(M_*^{\text{gal}})$, and then separately examine the behavior of each. As Figure 7 shows, when $\sigma_c \gtrsim 100 \text{ km s}^{-1}$ stellar mass does not help to reduce the scatter in pitch angle, but in the low- σ_c regime more massive galaxies tend to have smaller pitch angle, consistent with the empirical relation found in Section 4.2. Thus, galaxy mass can account for part of the scatter in pitch angle.

The $\varphi - M_*^{\text{gal}}$ relation and the $\varphi - \sigma_c$ relation are actually projections of a stronger three-parameter relation involving φ , M_*^{gal} , and σ_c . Figure 10 plots $\log(M_*^{\text{gal}})$ against σ_c . To separate the data equally into five fan-shaped bins, numerically denoted 1 to 5, we scale the data by dividing them by $(\sigma_{c,\text{max}} - \sigma_{c,\text{min}})$ and $(\log M_{*,\text{max}}^{\text{gal}} - \log M_{*,\text{min}}^{\text{gal}})$ and then generate six radiant dotted lines in the scaled parameter space, with equal separation in orientation angle of 18° , originating from a reference point with maximum σ_c and minimum M_*^{gal} . The counterparts of the dotted lines in the original $(\sigma_c, \log M_*^{\text{gal}})$ space are shown in Figure 10. We calculate the mean and standard deviation of φ in each bin. The inset panel in Figure 10 shows the tendency of pitch angle progressively increasing from the

fifth bin ($\varphi = 9^\circ.3 \pm 2^\circ.0$) to the first bin ($\varphi = 26^\circ.0 \pm 6^\circ.0$). Our results suggest that when σ_c or M_*^{gal} is high, φ is mainly determined by σ_c , whereas when σ_c or M_*^{gal} is low, φ is mainly determined by M_*^{gal} . Figure 10 can explain the behavior of the $\varphi - M_*^{\text{gal}}$ and $\varphi - \sigma_c$ relations. In the high-mass regime, the scatter in φ is large at a given M_*^{gal} (Figure 5b) because σ_c is high ($\sim 130 - 210 \text{ km s}^{-1}$) and φ is mainly dictated by σ_c . In the low- σ_c regime, the mean value of φ remains nearly constant with σ_c (Figure 7) because φ is mainly determined by M_*^{gal} instead of σ_c . Therefore, our results suggest that two primary parameters—central velocity dispersion and galaxy mass—synergistically determine spiral arm pitch angle.

4.3.4. Morphology of the Rotation Curve of the Central Region

The observed rotation curves can be grouped roughly qualitatively into several types according to their behavior in the central region (e.g., Keel 1993; Sofue et al. 1999). Kalinova et al. (2017) applied principal component analysis to quantitatively classify the rotation curves of the CALIFA galaxies. The coefficient of the first eigenvector PC_1 describes the morphology of the rotation curve of the central region. Galaxies with high PC_1 (> 0) have a high-amplitude, centrally peaked rotation curve that attains a sharp maximum near the center, followed by a dip and then a broad maximum of the disk component; those with low PC_1 (< 0) have a low-amplitude, slow-rising rotation curve that rises gradually from the center in a rigid-body fashion. As the coefficient PC_1 is a measure of both the shape and amplitude of the rotation curve, PC_1 simultaneously reflects the mass of the central component and the mass of the disk, especially for bulgeless galaxies. As expected from the $\varphi - \sigma_c - M_*^{\text{gal}}$ relation, φ shows a strong inverse correlation with PC_1 (Figure 11; $\rho = -0.66$).

In addition to baryonic mass, the shape and the amplitude of the rotation curve also reflect the mass distribution of dark matter in galaxies. Hence, the strong correlation between pitch angle and morphology of the central rotation curve also implies that dark matter content might help to shape spiral arms.

4.3.5. Shear rate

The strong correlation between pitch angle and shear rate Γ originally suggested by (Seigar et al. 2005, 2006) has not been substantiated by the recent study of Yu et al. (2018), who show that $\sim 1/3$ of the pitch angle measurements of Seigar et al. (2006) have been severely overestimated, as a consequence of which the correlation between φ and Γ is much weaker than pre-

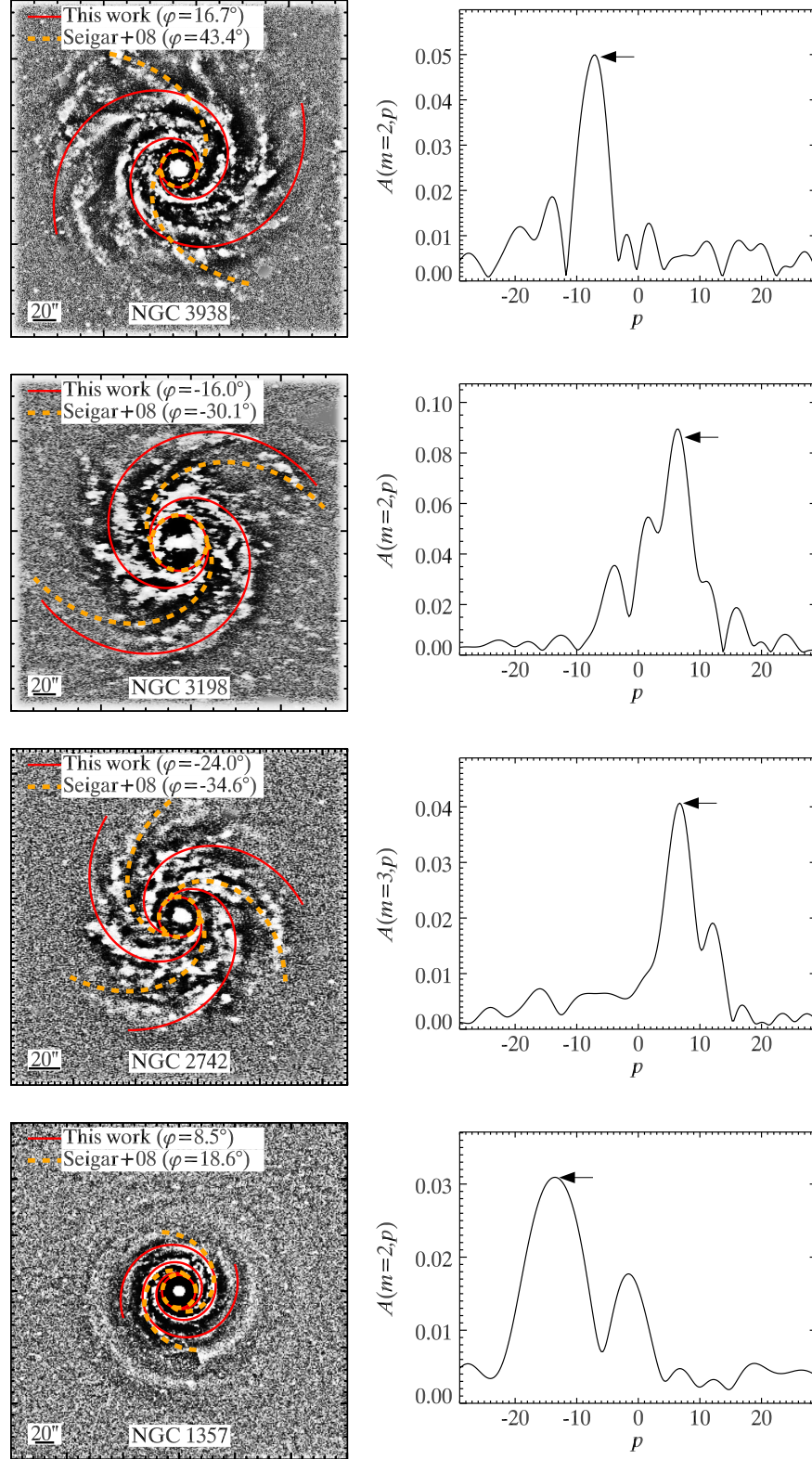


Figure 8. Illustration of our new measurements of pitch angle for four galaxies in common with the study of Seigar et al. (2008). (Left) Unsharp-masked image overplotted with synthetic arms with our pitch angle (red-solid curve) and that of Seigar et al. (2008; dashed-orange curve). (Right) Fourier spectra to derive the pitch angle, with an arrow indicating the peak chosen.

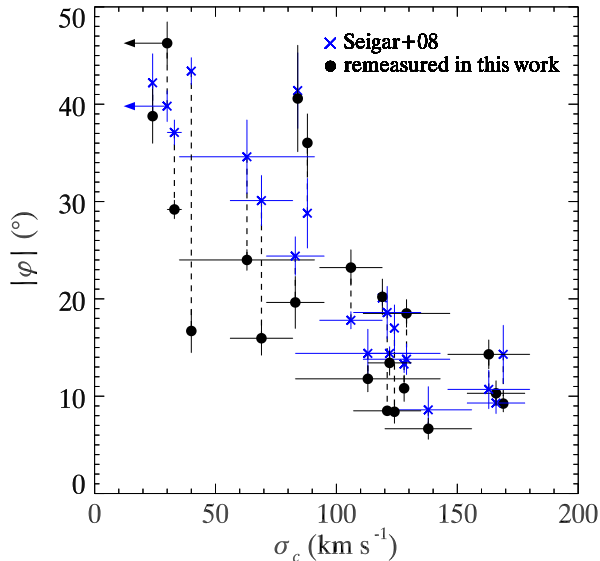


Figure 9. Correlation between pitch angle and σ_c . Blue crosses mark the results from Seigar et al. (2008), while black solid points represent our new measurements. Data points for the same galaxy are connected with a dashed line for comparison. Our new measurements show that there are objects with pitch angles $\sim 20^\circ$ at $\sigma_c \approx 50 \text{ km s}^{-1}$, making the trend very similar to that presented in Figure 7.

viously claimed². We reassess the relationship between φ and Γ in Figure 12. Pitch angle does have a tendency to decline with increasing Γ ($\rho = -0.49$), although the scatter is large. Two physical mechanisms may explain this behavior.

An association between φ and Γ was recently explored using numerical simulations by Grand et al. (2013) and Michikoshi & Kokubo (2014). N -body simulations of isolated stellar disks produce transient but recurrent local spiral arms (Carlberg & Freedman 1985; Bottema 2003; Sellwood 2011; Fujii et al. 2011; Grand et al. 2012a,b; Baba et al. 2013; D’Onghia et al. 2013). D’Onghia et al. (2013) argue that spiral arms originate from the dynamical response of a self-gravitating shearing disk to local density perturbations. Differential motion tends to stretch and break up the spiral arms locally. In regions where self-gravity dominates, the disk is locally overdense and generates

² It behooves us to note that we uncovered similar problems with the pitch angle measurements in Seigar et al. (2005). For example, these authors report $\varphi = 30^\circ 4 \pm 1.9$ for ESO 576–G51, but the Fourier spectra shown in their Figure 2 clearly demonstrate that its dominant $m = 2$ mode reaches its peak at $p \approx 6$, which corresponds to only $\varphi \approx 18^\circ$. Inspection of the Fourier spectra of other galaxies in their study (e.g., ESO 474–G33) reveals similar inconsistencies.

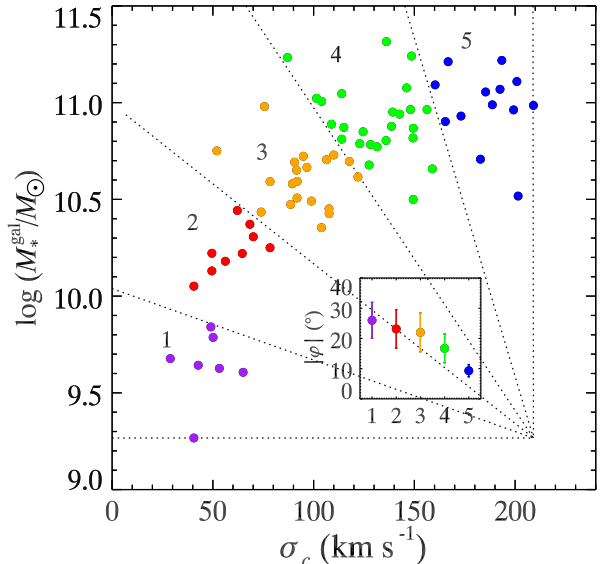


Figure 10. Galaxy stellar mass (M_*^{gal}) is plotted against central velocity dispersion (σ_c). The data are further separated into five fan-shaped bins, denoted by number of 1 (purple), 2 (red), 3 (orange), 4 (green), and 5 (blue). The mean value and standard deviation of pitch angle in each bin are shown in the inset panel: (1) $26^\circ 0 \pm 6^\circ 0$, (2) $23^\circ 1 \pm 6^\circ 4$, (3) $21^\circ 9 \pm 6^\circ 4$, (4) $16^\circ 7 \pm 4^\circ 7$, and (5) $9^\circ 3 \pm 2^\circ 0$. Our results suggest that when σ_c or M_*^{gal} is high, the pitch angle is mainly determined by σ_c , while when σ_c or M_*^{gal} is low, the pitch angle is mainly determined by M_*^{gal} .

arm segments, which reconnect and make up the spiral arms. The simulations of Grand et al. (2013) and Michikoshi & Kokubo (2014), marked by green crosses and blue triangles in Figure 12, share the same general tendency for φ to decline with increasing Γ . However, a systematic offset can be clearly seen. For a given shear rate, the predicted pitch angles are larger than the observed values, typically by $\Delta\varphi \gtrsim 8^\circ$, especially at the low- Γ end. This implies that, in terms of arm morphology, N -body simulations cannot yet generate realistic spiral arms even if the resolution of the simulations is very high.

Swing amplification (Julian & Toomre 1966; Goldreich & Tremaine 1978; Toomre 1981) is a mechanism of amplifying spiral arms when a leading spiral pattern rotates to a trailing one due to the shear in a differentially rotating disk. Swing amplification theory is reasonably consistent N -body simulations in terms of the predicted number of arms, which is approximately inversely proportional to the mass fraction of the disk component (Carlberg & Freedman 1985; Bottema 2003; Fujii et al. 2011; D’Onghia et al. 2013), and in terms of the relationship between the shear rate of the rotation curve

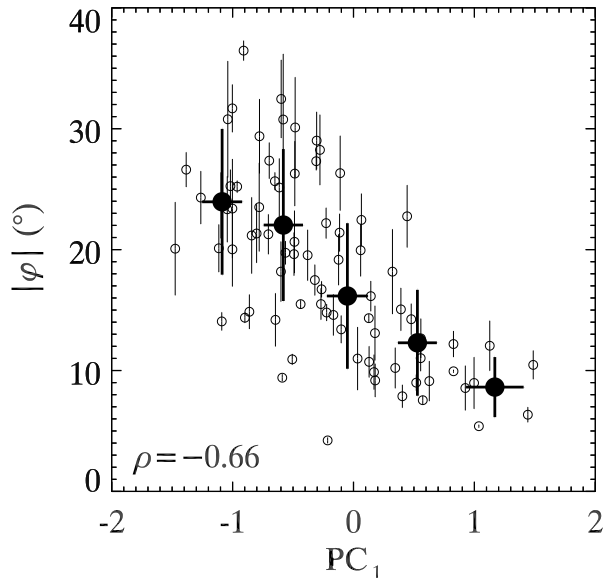


Figure 11. The pitch angle shows a strong inverse correlation with PC_1 . The data points are grouped into five equal bins of PC_1 . The solid black points and their associated error bars mark the mean value and standard deviation of the data in each bin. PC_1 reflects the morphology of the rotation curve in the central region. Galaxies with high PC_1 (> 0) have a high-amplitude, centrally peaked rotation curve that attains a sharp maximum near the center, followed by a dip and then a broad maximum of the disk component; those with low PC_1 (< 0) have a low-amplitude, slow-rising rotation curve that rises gently from the center in a rigid-body fashion. The Pearson’s correlation coefficient, ρ , is shown on the bottom-left corner.

and the pitch angle of the simulated spirals (Grand et al. 2013; Michikoshi & Kokubo 2014).

Michikoshi & Kokubo (2014) derived a theoretical relation between φ and Γ in the context of swing amplification theory. We give a brief summary here. We consider a material arm that swings from leading to trailing due to differential motion. The pitch angle evolves as (e.g., Binney & Tremaine 2008)

$$\tan \varphi = \frac{1}{2At}, \quad (3)$$

where A is the first Oort constant and $t = 0$ means that the arm extends radially outward across the disk ($\varphi = 90^\circ$). In the simulations of Michikoshi & Kokubo (2014), Toomre’s Q parameter increases rapidly and exceeds 1.5 for $\Gamma \gtrsim 0.5$. In the linear approximation of swing amplification theory, if $Q > 1.5$, the maximum amplification is reached at $t_{\max} \simeq 3.5/\kappa$, where κ is the epicyclic frequency. They interpret the most amplified short wave as the spiral structures observed in their sim-

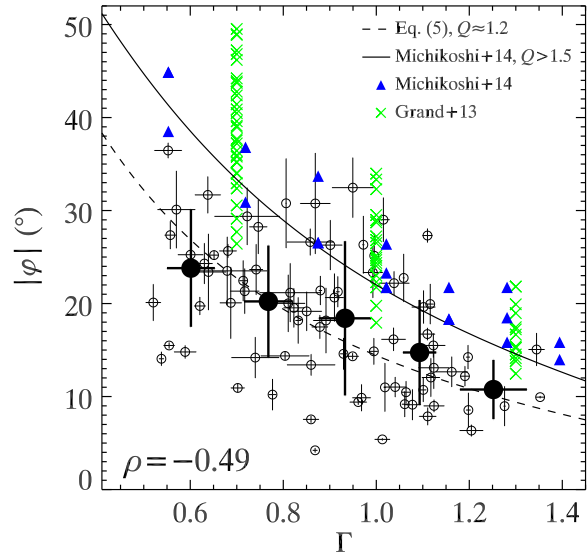


Figure 12. Comparison between pitch angle and shear rate. Our measurements are plotted as small open black points, with large solid black points denoting the mean and associated standard deviation for five equal bins in Γ . The results from N -body simulations of Grand et al. (2013) and Michikoshi & Kokubo (2014) are plotted as green crosses and blue triangles, respectively. The black solid curve traces the theoretical prediction of swing amplification theory, given by Michikoshi & Kokubo (2014), assuming $Q > 1.5$. The dashed curve denotes the prediction for $Q \approx 1.2$ (Eq. (5)). The Pearson’s correlation coefficient, ρ , is shown on the bottom-left corner.

ulation. Combined with $\Gamma = \frac{2A}{\Omega}$, the relation between pitch angle and shear rate becomes (their Eq. 15)

$$\tan \varphi = \frac{2\sqrt{4-2\Gamma}}{\Gamma}. \quad (4)$$

This is indicated by the solid line in Figure 12. The prediction from swing amplification theory is quantitatively consistent with the results from N -body simulations. Note that the predicted pitch angle for a given shear rate is still higher than our measurements (by $\sim 8^\circ$). This is because Eq. (4) assumes $Q > 1.5$, which is indeed the case for the simulated spiral galaxies of Michikoshi & Kokubo (2014). However, as suggested by Bertin et al. (1989a), because of self-regulation of gas content, Toomre’s Q parameter in the outer regions of galactic disks should be close to unity. On the other hand, Q may be substantially larger in the central regions of galaxies because of the presence of a bulge. Considering both the effects of the disk and the bulge, if Q is constrained to ~ 1.2 , we estimate from Figure 7 of Michikoshi & Kokubo (2014) that $t_{\max} \approx 5.5/\kappa$. For $Q \approx 1.2$, we obtain, from swing amplification theory,

$$\tan \varphi = \frac{2}{11} \frac{\sqrt{4 - 2\Gamma}}{\Gamma}. \quad (5)$$

This revised relation, presented as the dashed curve in Figure 12, is now consistent with our observational results. Our results have two important implications. First, if swing amplification theory is the correct framework to explain spiral structures in galaxies, then Toomre’s Q should be roughly 1.2. And second, to generate more realistic spiral arms, simulations may need an effective cooling mechanism for the disk, perhaps by including the effects of gas, to lower Toomre’s Q .

In the framework in which spiral structure constitute transient material arms, the shape of the arms should reflect the effects of differential rotation alone. Although we present some evidence supporting this picture, the existence of other stronger empirical relationships between pitch angle and σ_c or PC_1 , which have statistically stronger correlation coefficients, probably rules out the transient material arms scenario.

A more compelling, alternative explanation for the relationship between pitch angle and shear rate comes from density wave theory. As the shape of the rotation curve depends on the distribution of mass, the shear rate reflects the mass concentration. Consequently, the inverse correlation between φ and Γ is qualitatively consistent with the expectations of density wave models (Lin & Shu 1964; Roberts et al. 1975; Bertin et al. 1989a,b). The predicted relation between φ and Γ is consistent with our observed $\varphi - C_{28}$ relation (Figure 5b).

5. SUMMARY AND CONCLUSIONS

After more than half a century of research, the physical origin of spiral arms in galaxies is still a topic of debate (for a review, see Dobbs & Baba 2014). The pioneering work of Kennicutt (1981) systematically established the dependence of spiral arm pitch angle (φ) on galaxy properties, but there have been only a handful of quantitative follow-up studies since (Ma 2002; Seigar et al. 2005, 2006, 2008; Kendall et al. 2011, 2015; Davis et al. 2015; Hart et al. 2017). The CALIFA survey of nearby galaxies provides a good opportunity to revisit this problem, given the plethora of relevant ancillary measurements available for the sample, including luminosity, stellar mass, photometric decomposition, and kinematics (Walcher et al. 2014; Sánchez et al. 2016; Falcón-Barroso et al. 2017; Sánchez et al. 2017; Méndez-Abreu et al. 2017; Catalán-Torrecilla et al. 2017; Gilhuly & Courteau 2018). Because of the low redshift of the sample, SDSS images are adequate to

resolve the spiral structure of the galaxies (Yu et al. 2018). This paper uses SDSS r -band images to perform a detailed analysis of the spiral structure of the 79 relatively face-on CALIFA spiral galaxies with available published rotation curves. We aim to systematically examine the correlation between spiral arm pitch angle and other galaxy properties to investigate the physical origin of spiral arms.

As implicit in the Hubble classification system (Hubble 1926; Sandage 1961), we confirm that spiral arms become more open from early to late-type galaxies. The pitch angle of spiral arms decreases with brighter absolute magnitude, larger stellar mass (total, bulge, or disk), and higher concentration (C_{28}), although all these correlations contain significant scatter. Pitch angle is also correlated with B/T . For a given M_*^{gal} , galaxies with higher C_{28} have tighter spiral arms. Similarly, for a given C_{28} , more massive galaxies have tighter spirals. These trends are consistent with the density wave theory for spirals, which predicts that pitch angle decreases with higher mass concentration (Roberts et al. 1975) and larger surface density (Hozumi 2003). We also find a strong correlation between pitch angle and central stellar velocity dispersion: $\sigma_c \gtrsim 100 \text{ km s}^{-1}$, φ decreases with increasing σ_c with small scatter, whereas φ remains roughly constant for $\sigma_c \lesssim 100 \text{ km s}^{-1}$. This behavior has important implications. We show that φ is mainly determined by σ_c for massive galaxies, while the primary determinant of φ becomes M_*^{gal} for less massive galaxies. We then demonstrate that the $\varphi - M_*^{\text{gal}}$ and $\varphi - \sigma_c$ relations are projections of higher dimensional relationship between φ , M_*^{gal} , and σ_c .

Spiral arm pitch angle is closely connected to the morphology of the central rotation curve, quantified by PC_1 , the coefficient of the first eigenvector from principal component analysis. Galaxies with centrally peaked rotation curves tend to have tight arms; those with slow-rising rotation curves tend to have loose arms. As PC_1 reflects both the mass of the central component and of the disk, especially for bulgeless galaxies, the connection between pitch angle and the morphology of the central rotation curve is consistent with the $\varphi - \sigma_c - M_*^{\text{gal}}$ relation.

We do not confirm the strong connection between pitch angle and galactic shear rate (Γ) found in previous studies. N -body simulations (e.g., Grand et al. 2013; Michikoshi & Kokubo 2014), while generally successful in reproducing the qualitative dependence between φ and Γ , systematically overpredicts φ at fixed Γ . The observed inverse correlation between φ and Γ can be interpreted in the context of transient material arms obeying swing amplification theory, provided that

Toomre's $Q \approx 1.2$. In this scenario, the shape of the spiral arms reflects the effects of differential rotation alone.

Differential rotation, however, is likely not the primary determinant of spiral arm pitch angle, as the empirical correlation between φ and Γ is not as strong as those between φ and σ_c or PC_1 . The totality of the ev-

idence places greater weight on the density wave theory for the origin of spiral arms in galaxies.

This work was supported by the National Key R&D Program of China (2016YFA0400702) and the National Science Foundation of China (11473002, 11721303). We are grateful to an anonymous referee for helpful feedback.

REFERENCES

- Baba, J., Saitoh, T. R., & Wada, K. 2013, *ApJ*, 763, 46
- Bertin, G., & Lin, C. C. 1996, *Spiral Structure in Galaxies a Density Wave Theory* (Cambridge, MA: MIT Press)
- Bertin, G., Lin, C. C., Lowe, S. A., & Thurstans, R. P. 1989a, *ApJ*, 338, 78
- Bertin, G., Lin, C. C., Lowe, S. A., & Thurstans, R. P. 1989b, *ApJ*, 338, 104
- Binney, J., & Tremaine, S. 2008, *Galactic Dynamics* (2nd ed.; Princeton, NJ: Princeton Univ. Press)
- Block, D. L., Bertin, G., Stockton, A., et al. 1994, *A&A*, 288, 365
- Block, D. L., & Puerari, I. 1999, *A&A*, 342, 627
- Bottema, R. 2003, *MNRAS*, 344, 358
- Cappellari, M. 2008, *MNRAS*, 390, 71
- Cappellari, M., & Emsellem, E. 2004, *PASP*, 116, 138
- Cardelli, J. A., Clayton, G. C., & Mathis, J. S. 1989, *ApJ*, 345, 245
- Carlberg, R. G., & Freedman, W. L. 1985, *ApJ*, 298, 486
- Catalán-Torrecilla, C., Gil de Paz, A., Castillo-Morales, A., et al. 2017, *ApJ*, 848, 87
- Davis, B. L., Berrier, J. C., Shields, D. W., et al. 2012, *ApJS*, 199, 33
- Davis, B. L., Kenefick, D., Kenefick, J., et al. 2015, *ApJL*, 802, L13
- Davis, D. R., & Hayes, W. B. 2014, *ApJ*, 790, 87
- Dobbs, C., & Baba, J. 2014, *PASA*, 31, e035
- D'Onghia, E., Vogelsberger, M., & Hernquist, L. 2013, *ApJ*, 766, 34
- Elmegreen, D. M., Chromey, F. R., Bissell, B. A., & Corrado, K. 1999, *AJ*, 118, 2618
- Elmegreen, D. M., & Elmegreen, B. G. 2014, *ApJ*, 781, 11
- Faber, S. M., & Jackson, R. E. 1976, *ApJ*, 204, 668
- Falcón-Barroso, J., Lyubenova, M., van de Ven, G., et al. 2017, *A&A*, 597, A48
- Fujii, M. S., Baba, J., Saitoh, T. R., et al. 2011, *ApJ*, 730, 109
- Gao, H., & Ho, L. C. 2017, *ApJ*, 845, 114
- Gilhuly, C., & Courteau, S. 2018, *MNRAS*, 477, 845
- Gittins, D. M., & Clarke, C. J. 2004, *MNRAS*, 349, 909
- Goldreich, P., & Tremaine, S. 1978, *ApJ*, 222, 850
- Gonzalez, R. A., & Graham, J. R. 1996, *ApJ*, 460, 651
- Grand, R. J. J., Kawata, D., & Cropper, M. 2012, *MNRAS*, 426, 167
- Grand, R. J. J., Kawata, D., & Cropper, M. 2012, *MNRAS*, 421, 1529
- Grand, R. J. J., Kawata, D., & Cropper, M. 2013, *A&A*, 553, A77
- Grosbøl, P., & Patsis, P. A. 1998, *A&A*, 336, 840
- Grosbøl, P., Patsis, P. A., & Pompei, E. 2004, *A&A*, 423, 849
- Hart, R. E., Bamford, S. P., Hayes, W. B., et al. 2017, *MNRAS*, 472, 2263
- Ho, L. C. 2007, *ApJ*, 668, 94
- Ho, L. C., Li, Z.-Y., Barth, A. J., Seigar, M. S., & Peng, C. Y. 2011, *ApJS*, 197, 21
- Hozumi, S. 2003, in *Galaxies and Chaos*, ed. G. Contopoulos & N. Voglis (Lecture Notes in Physics, Vol. 626; Berlin: Springer), 380
- Hubble, E. P. 1926, *ApJ*, 64,
- Iye, M., Okamura, S., Hamabe, M., & Watanabe, M. 1982, *ApJ*, 256, 103
- Julian, W. H., & Toomre, A. 1966, *ApJ*, 146, 810
- Kalinova, V., Colombo, D., Rosolowsky, E., et al. 2017, *MNRAS*, 469, 2539
- Kalnajs, A. J. 1975, *La Dynamique des galaxies spirales*, 241, 103
- Keel, W. C. 1993, *AJ*, 106, 1771
- Kendall, S., Clarke, C., & Kennicutt, R. C. 2015, *MNRAS*, 446, 4155
- Kendall, S., Kennicutt, R. C., & Clarke, C. 2011, *MNRAS*, 414, 538
- Kennicutt, R. C., Jr. 1981, *AJ*, 86, 1847
- Kennicutt, R. C., Jr., & Hodge, P. 1982, *ApJ*, 253, 101
- Kormendy, J., & Ho, L. C. 2013, *ARA&A*, 51, 511
- Kormendy, J., & Illingworth, G. 1983, *ApJ*, 265, 632
- Kormendy, J., & Kennicutt, R. C., Jr. 2004, *ARA&A*, 42, 603

- Krakow, W., Huntley, J. M., & Seiden, P. E. 1982, *AJ*, 87, 203
- Lin, C. C., & Shu, F. H. 1964, *ApJ*, 140, 646
- Ma, J. 2002, *A&A*, 388, 389
- Martínez-García, E. E. 2012, *ApJ*, 744, 92
- Martínez-García, E. E., & González-Lópezlira, R. A. 2011, *ApJ*, 734, 122
- Martínez-García, E. E., & González-Lópezlira, R. A. 2013, *ApJ*, 765, 105
- Martínez-García, E. E., González-Lópezlira, R. A., & Bruzual A., G. 2009, *ApJ*, 694, 512
- Martínez-García, E. E., Puerari, I., Rosales-Ortega, F. F., et al. 2014, *ApJL*, 793, L19
- Méndez-Abreu, J., Ruiz-Lara, T., Sánchez-Menguiano, L., et al. 2017, *A&A*, 598, A32
- Michikoshi, S., & Kokubo, E. 2014, *ApJ*, 787, 174
- Morgan, W. W. 1958, *PASP*, 70, 364
- Morgan, W. W. 1959, *PASP*, 71, 394
- Paturel, G., Petit, C., Prugniel, P., et al. 2003, *A&A*, 412, 45
- Puerari, I. 1993, *PASP*, 105, 1290
- Puerari, I., & Dottori, H. A. 1992, *A&AS*, 93, 469
- Roberts, W. W., Jr., Roberts, M. S., & Shu, F. H. 1975, *ApJ*, 196, 381
- Sánchez, S. F., Kennicutt, R. C., Gil de Paz, A., et al. 2012, *A&A*, 538, A8
- Sánchez, S. F., Pérez, E., Sánchez-Blázquez, P., et al. 2016, *RMxAA*, 52, 21
- Sánchez, S. F., Pérez, E., Sánchez-Blázquez, P., et al. 2016, *RMxAA*, 52, 171
- Sánchez, S. F., Barrera-Ballesteros, J. K., Sánchez-Menguiano, L., et al. 2017, *MNRAS*, 469, 2121
- Sandage, A. 1961, Washington: Carnegie Institution, 1961,
- Schlafly, E. F., & Finkbeiner, D. P. 2011, *ApJ*, 737, 103
- Seigar, M. S., Block, D. L., Puerari, I., Chorney, N. E., & James, P. A. 2005, *MNRAS*, 359, 1065
- Seigar, M. S., Bullock, J. S., Barth, A. J., & Ho, L. C. 2006, *ApJ*, 645, 1012
- Seigar, M. S., & James, P. A. 1998, *MNRAS*, 299, 685
- Seigar, M. S., Kennefick, D., Kennefick, J., & Lacy, C. H. S. 2008, *ApJL*, 678, L93
- Sellwood, J. A. 2011, *MNRAS*, 410, 1637
- Sofue, Y., Tutui, Y., Honma, M., et al. 1999, *ApJ*, 523, 136
- Thornley, M. D. 1996, *ApJL*, 469, L45
- Thornley, M. D., & Mundy, L. G. 1997, *ApJ*, 484, 202
- Toomre, A. 1981, in *Structure and Evolution of Normal Galaxies*, ed. S. M. Fall & D. Lynden-Bell (Cambridge: Cambridge Univ. Press), 111
- Walcher, C. J., Wisotzki, L., Bekeraité, S., et al. 2014, *A&A*, 569, A1
- Whitmore, B. C., & Kirshner, R. P. 1981, *ApJ*, 250, 43
- York, D. G., Adelman, J., Anderson, J. E., Jr., et al. 2000, *AJ*, 120, 1579
- Yu, S.-Y., & Ho, L. C. 2018, *ApJ*, in press (arXiv:1810.08979)
- Yu, S.-Y., Ho, L. C., Barth, A. J., & Li, Z.-Y. 2018, *ApJ*, 862, 13